Electronic Supplementary Material (ESI) for Journal of Materials Chemistry

Supporting Information

Diazaboroles with quinone units: hydrogen bonding network and n-type FETs involving a three-coordinate boron atom

Jun-ichi Nishida,[a] Tomohiro Fujita,[a] Yoshihide Fujisaki,[b] Shizuo Tokito[b] and Yoshiro Yamashita*[a]

[a]Department of Electronic Chemistry, Interdisciplinary Graduate School of Science and Engineering, Tokyo Institute of Technology, Nagatsuta, Midori-ku, Yokohama 226-8502, *Japan*.

[b]NHK Science and Technical Research Laboratories, Kinuta, Setagaya-ku, Tokyo 157-8510, *Japan*.

E-mail: yoshiro@echem.titech.ac.jp

Contents

1. FT-IR data (ATR method)
2. NMR data
3. X-ray structure analysis
4. UV-Vis data
5. Redox potentials
6. DFT calculations
7. FET characteristics
8. XRD patterns
9. AFM measurements

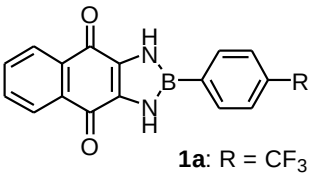

1a: R = CF_3
1b: R = *t*-Bu

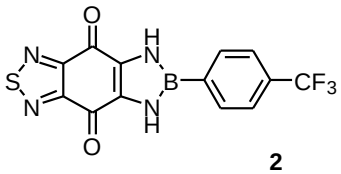

2

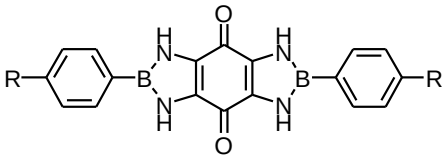

3a: R = H
3b: R = CF_3
3c: R = Ph
3d: R = *t*-Bu

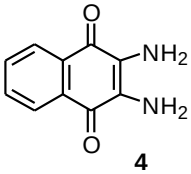

4

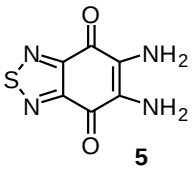

5

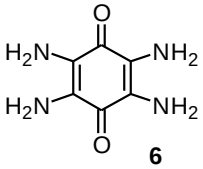

6

Lists of compounds

1. FT-IR data (ATR method: ZnSe)

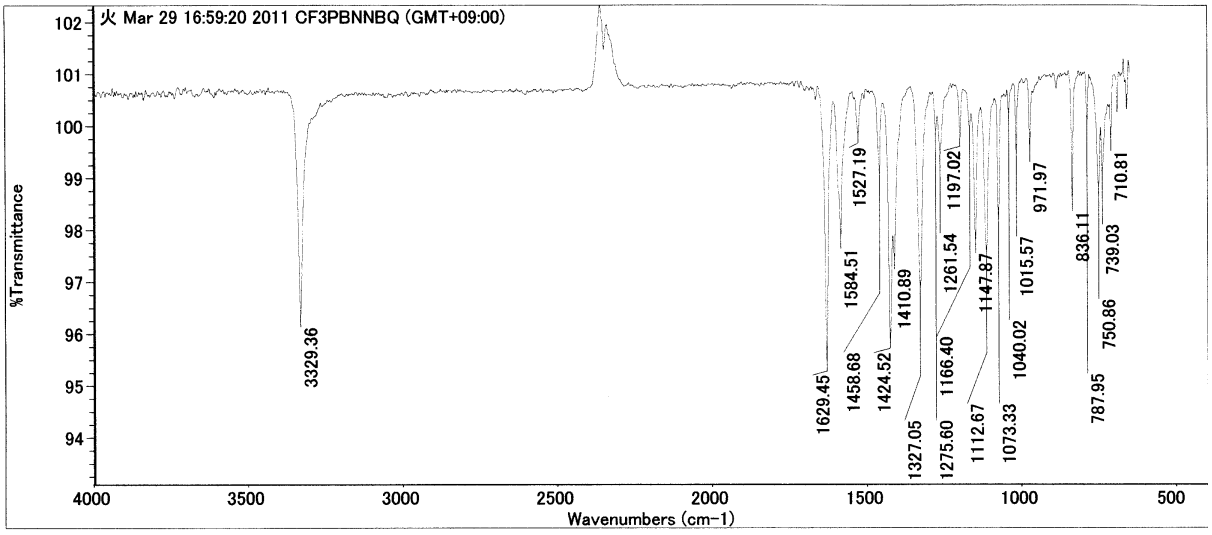

Figure S1-1. FT-IR data of **1a**.

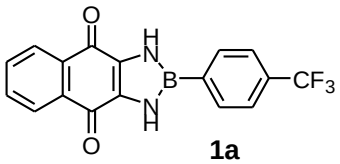

1a

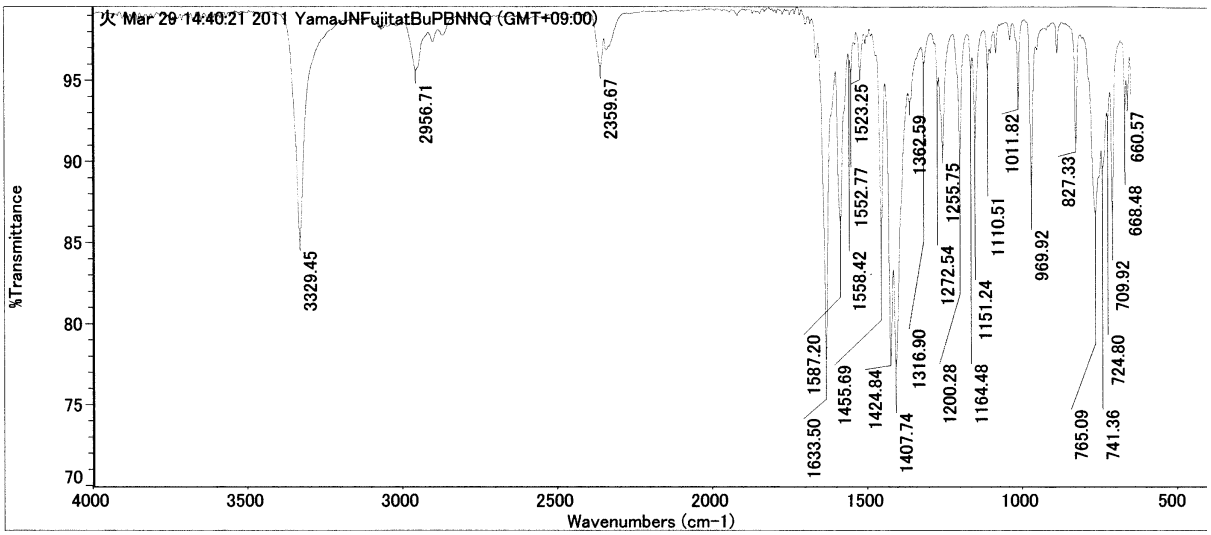

Figure S1-2. FT-IR data of **1b**.

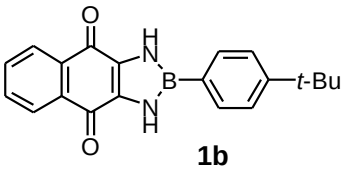

1b

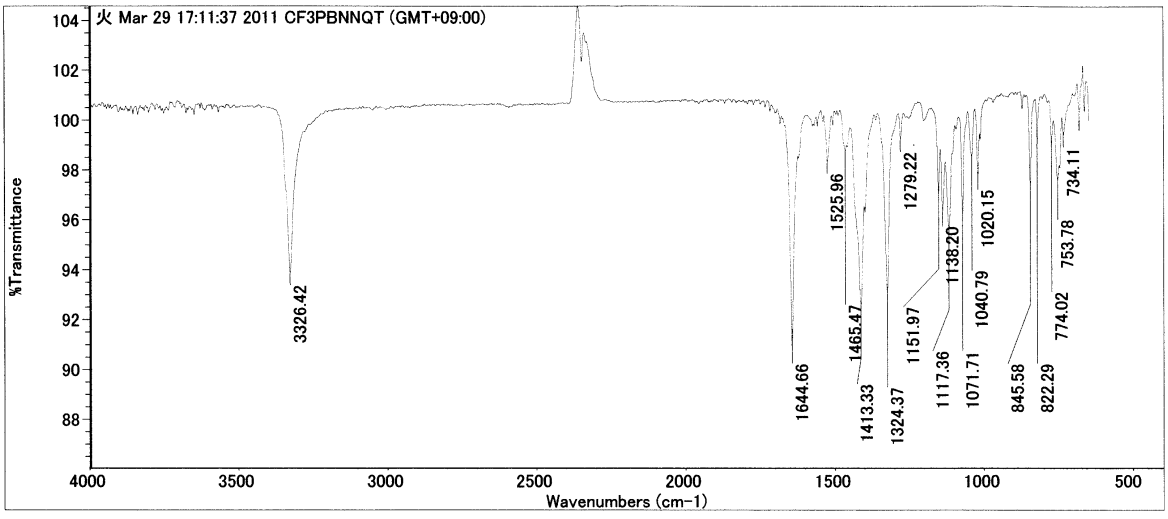

Figure S1-3. FT-IR data of **2**.

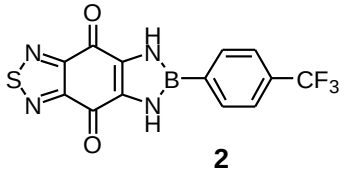

2

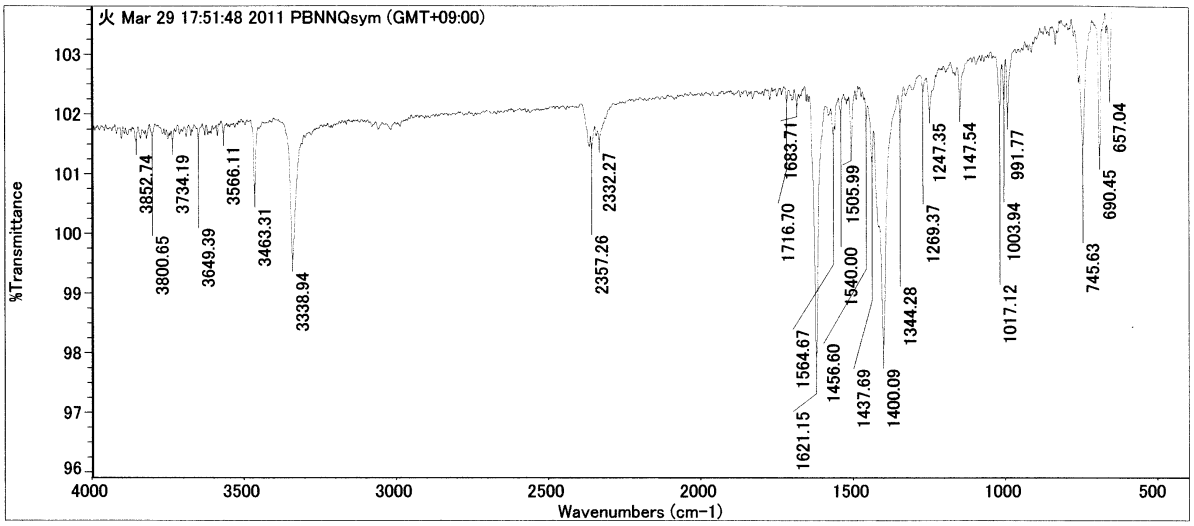

Figure S1-4. FT-IR data of **3a**.

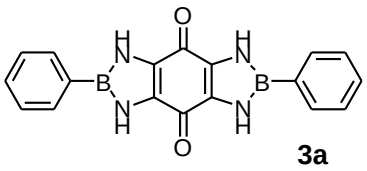

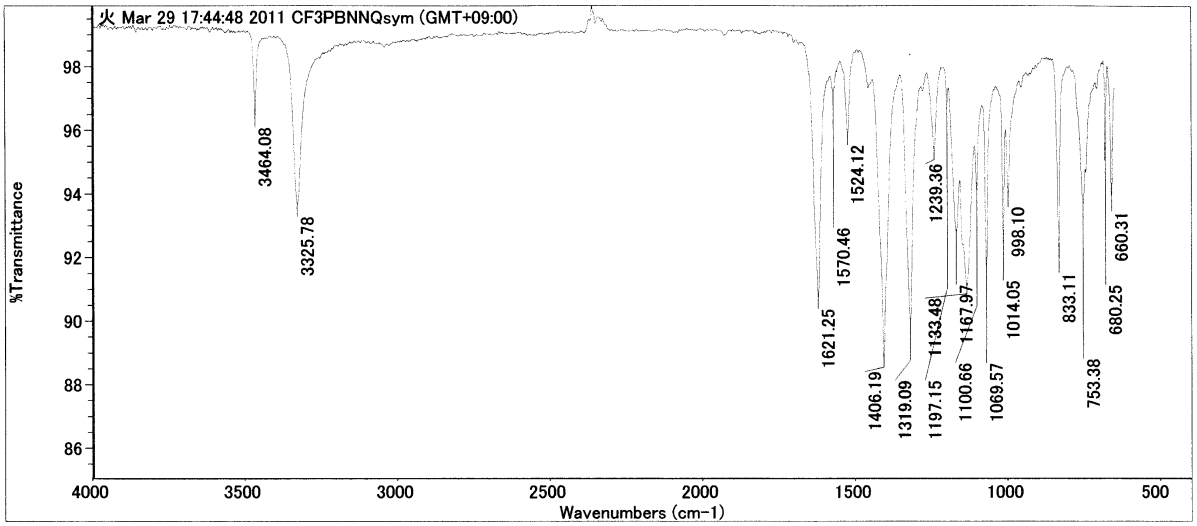

Figure S1-5. FT-IR data of **3b**.

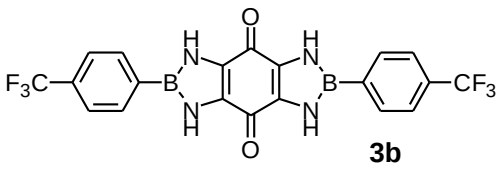

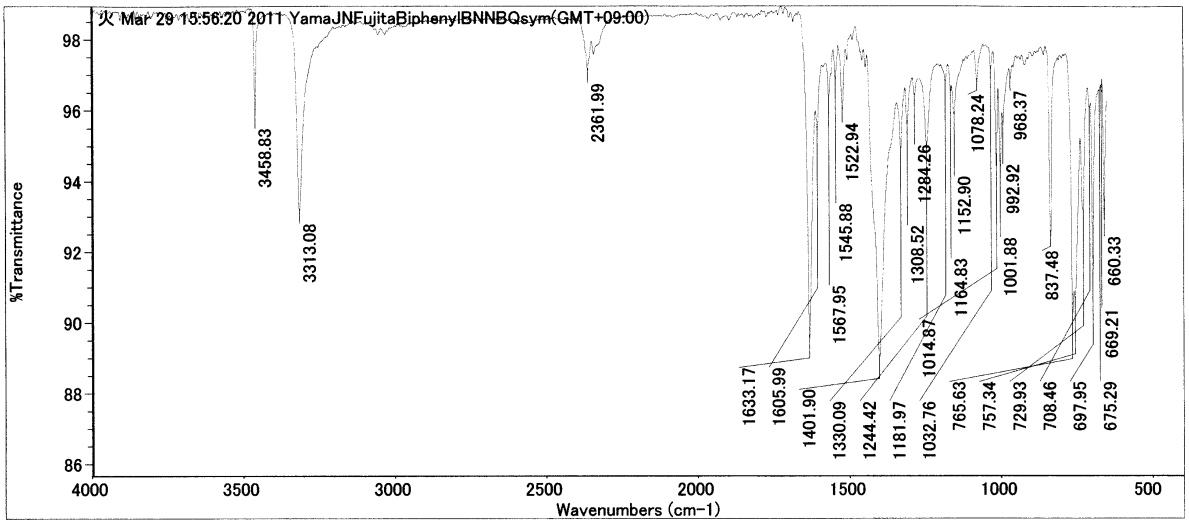

Figure S1-6. FT-IR data of **3c**.

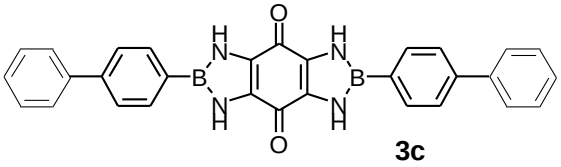

3c

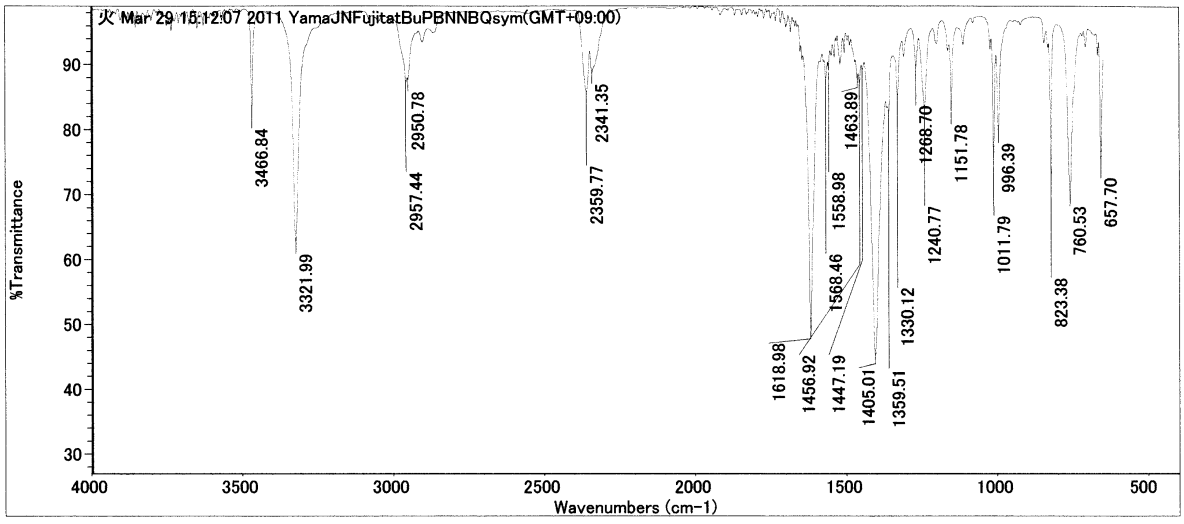

Figure S1-7. FT-IR data of **3d**.

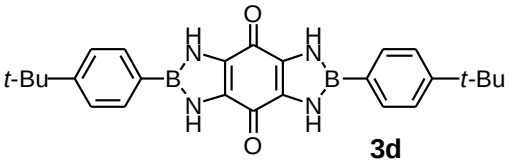

3d

2. NMR data (In DMSO: rt)

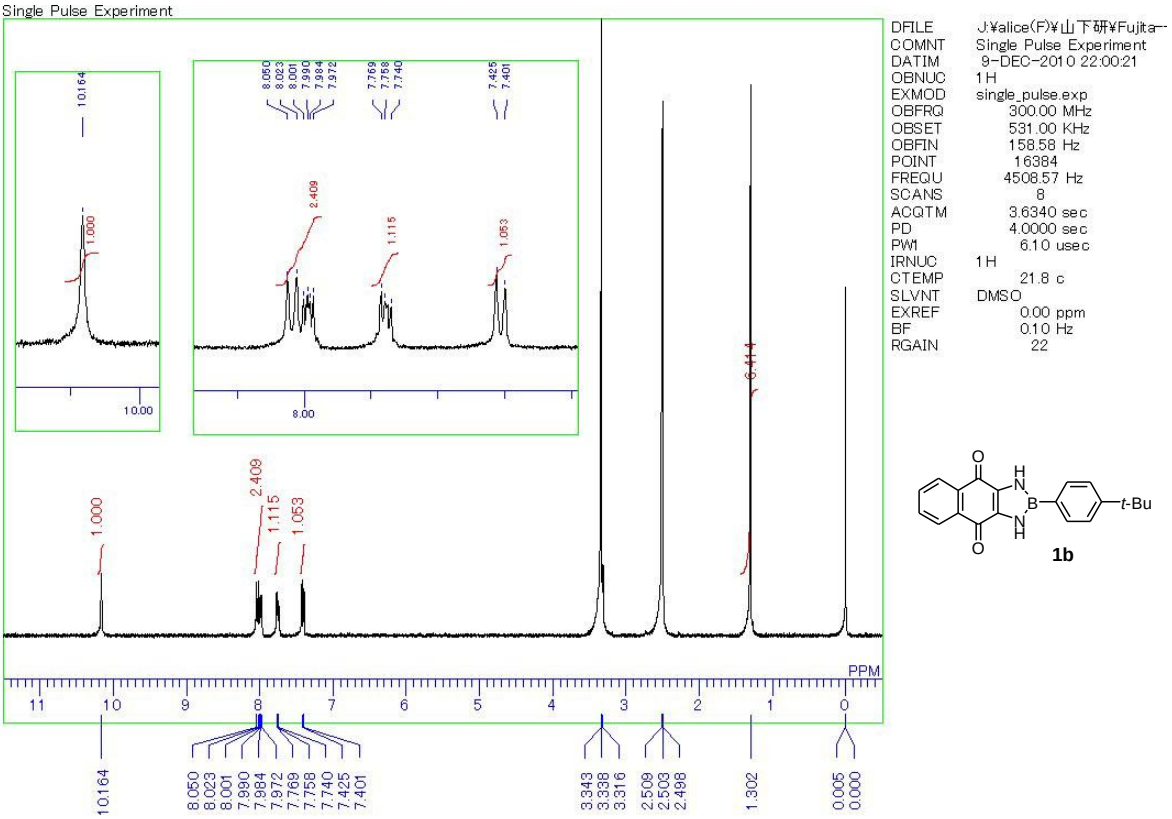

Figure S2-1. NMR data of *t*-butyl derivative **1b**.

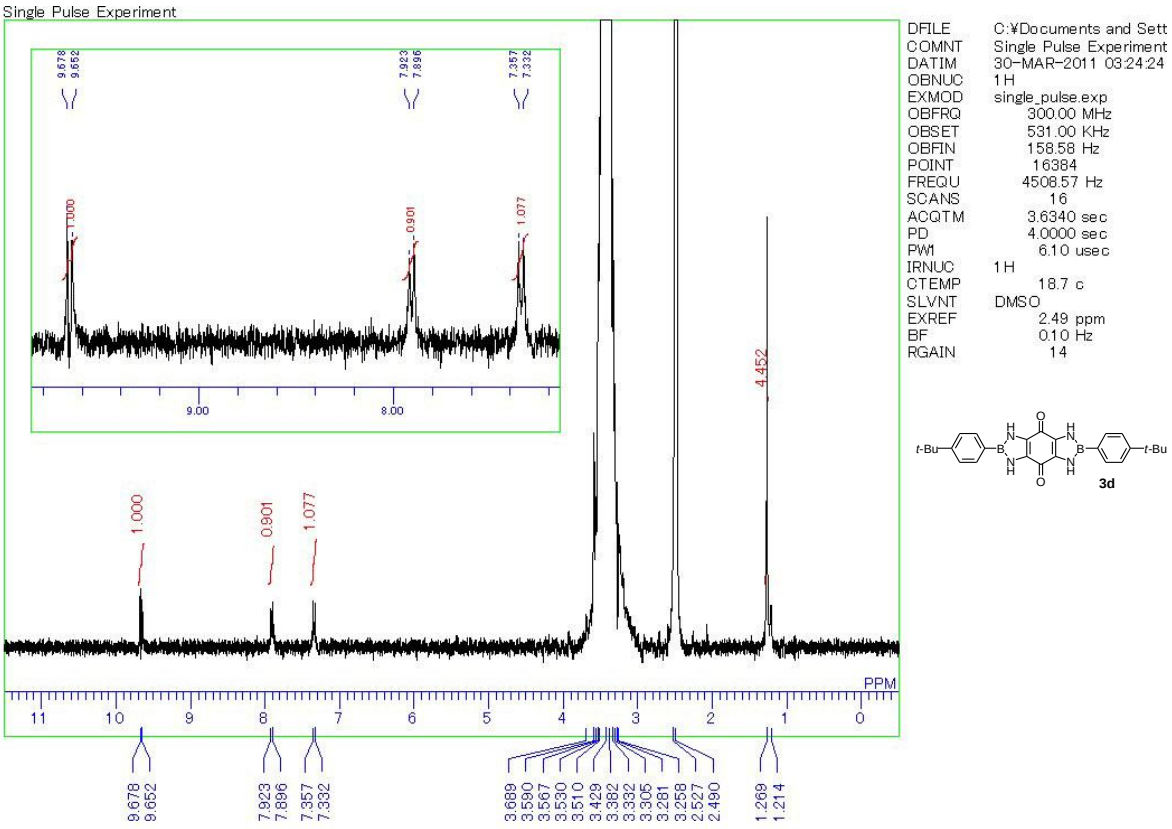

Figure S2-2. NMR data of *t*-butyl derivative **3d**.

3. X-ray analysis

X-ray measurement of single crystal of **1a** was carried out using a RAXIS-RAPID imaging plate diffractometer with Mo-Ka radiation (λ = 0.71075 Å) at −180.0 ˚C. The structure was solved by the direct method (SIR2004) and refined by the full-matrix least-squares method on F^2. The non-hydrogen atoms were refined anisotropically. Hydrogen atoms were refined using the riding model. Absorption correction was applied using an empirical procedure. All calculations were performed using the CrystalStructure crystallographic software package except for refinement, which was performed using SHELXL-97. **Crystal data for 1a**: $C_{17}H_{10}N_2O_2F_3B_2$, M = 342.08, red platelet, crystal dimensions 0.70 × 0.70 × 0.15 mm, triclinic, space group P-1, a = 5.5337(12), b = 7.9622(19), c = 16.321(3) Å, α = 101.835(6), β = 94.236(7), γ = 93.967(6), V = 699.3(3) Å^3, Z = 2, D_c = 1.625 g cm^{-3}, 6507 relections collected, 3115 independent (R_{int} = 0.049), GOF = 1.022, R_1 = 0.1265 (I>2.00σ(I)), wR_2 = 0.3359 for all reflections.

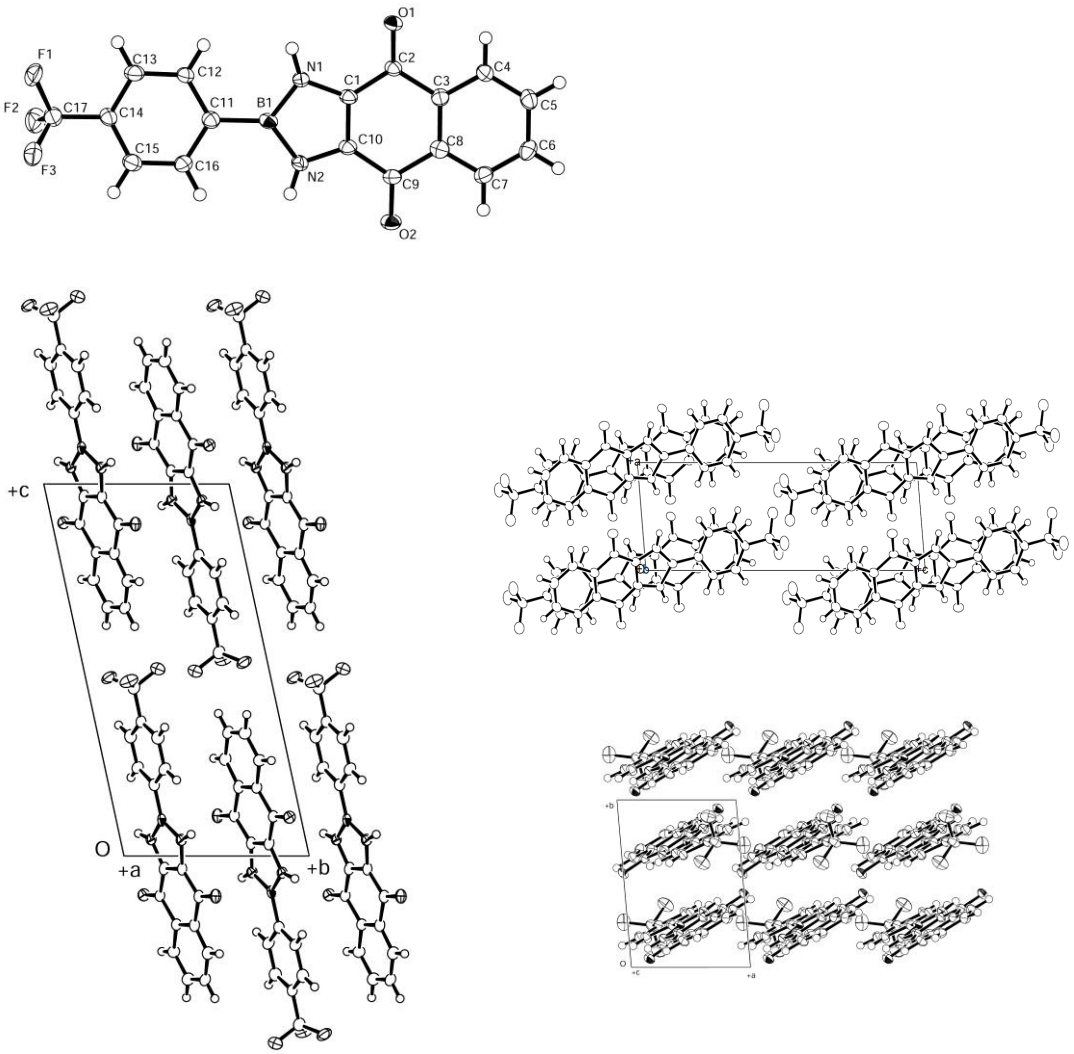

Figure S3. Crystal structures of compound **1a**.

4. UV-Vis data

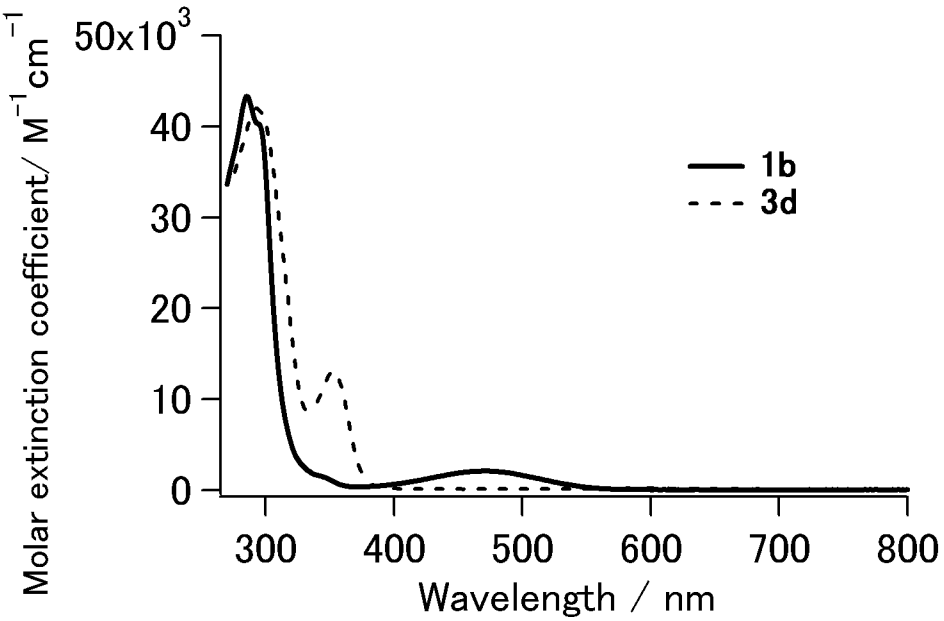

Figure S4-1. UV-Vis spectra of *t*-butyl derivatives **1b** and **3d** in DMF.

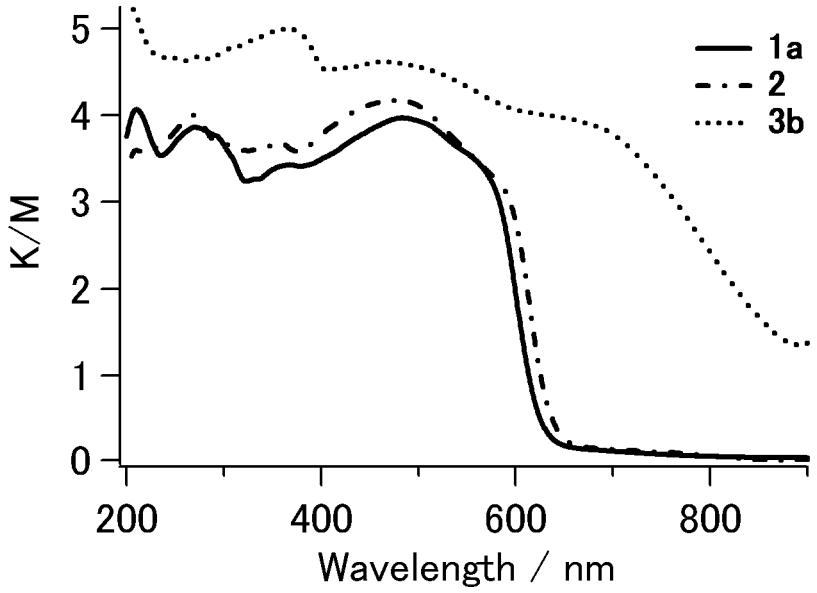

Figure S4-2. Reflection spectra of **1a**, **2** and **3b** in solid states after K-M transformation.

5. Redox potentials

(a)

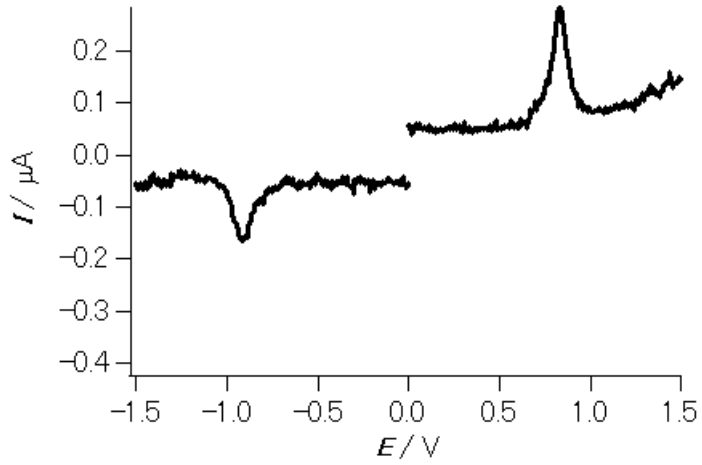

(b)

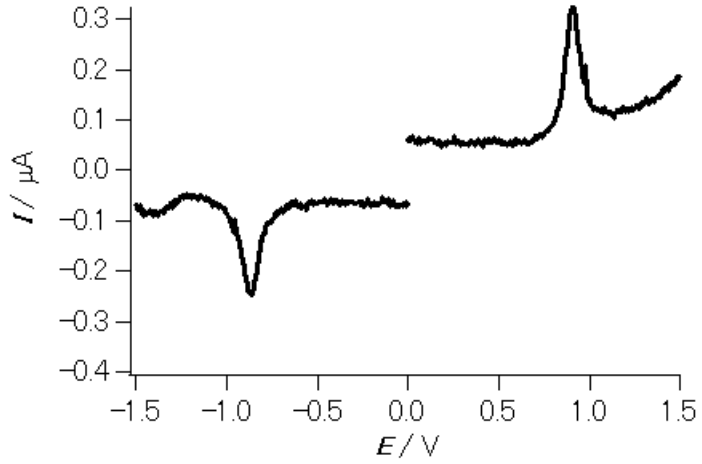

(c)

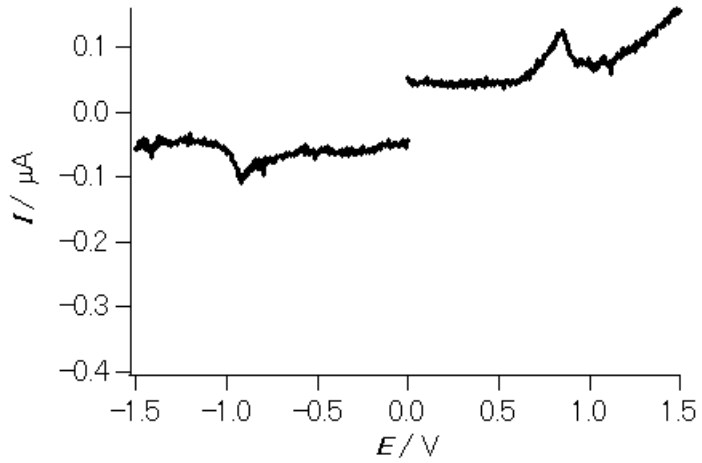

Figure S5. Differential pulse voltammograms of (a) **3a**, (b) **3b** and (c) **3c**. 0.1 M *n* -Bu_4NPF_6 in DMF, Pt electrode, scan rate 20 mV s^{-1}, V vs SCE.

6. DFT calculations

B3LYP/6-31G(d) level using the Gaussian program 03

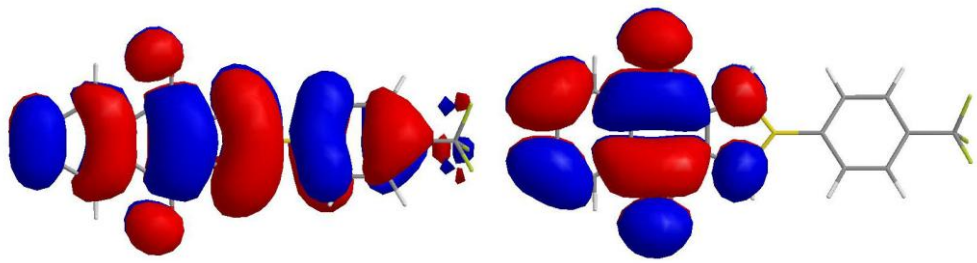

Figure S6-1. HOMO (6.15 eV: left) and LUMO (2.93 eV: right) of **1a**.

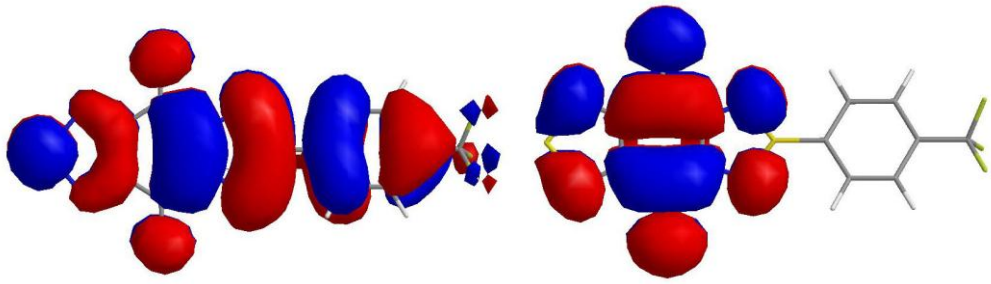

Figure S6-2. HOMO (6.53 eV: left) and LUMO (3.27 eV: right) of **2**.

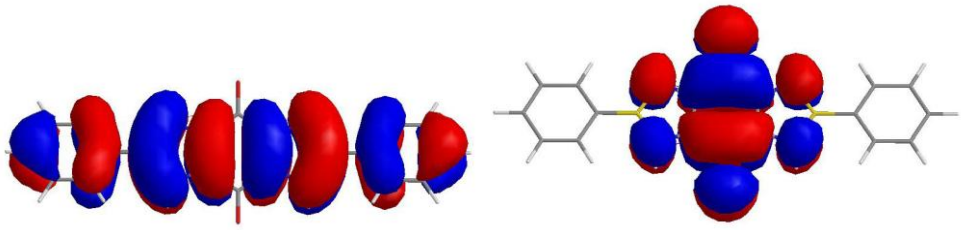

Figure S6-3. HOMO (5.34 eV: left) and LUMO (2.78 eV: right) of **3a**.

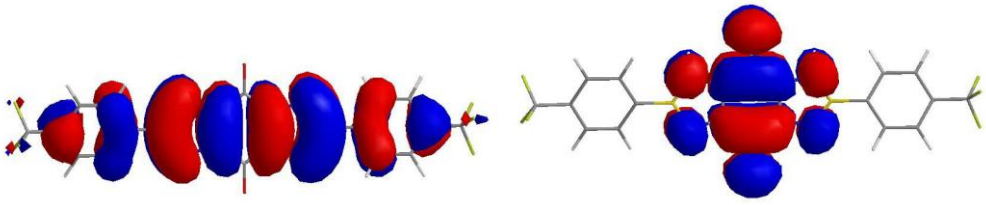

Figure S6-4. HOMO (5.74 eV: left) and LUMO (3.09 eV: right) of **3b**.

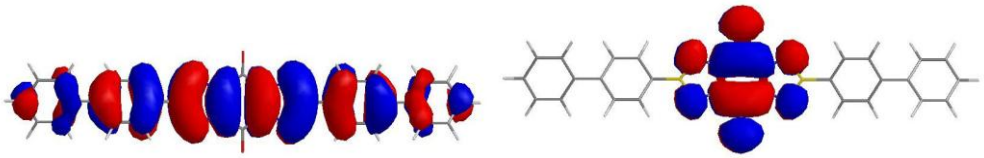

Figure S6-5. HOMO (5.30 eV: left) and LUMO (2.79 eV: right) of **3c**.

.

DFT calculations of the tautomeric forms of 1a

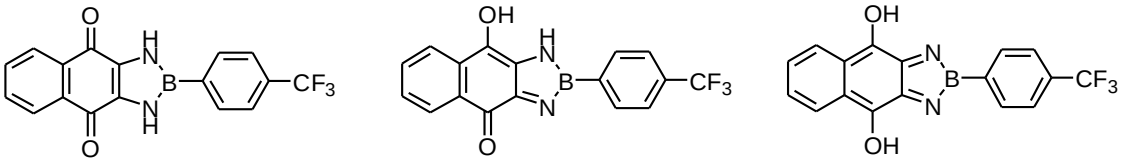

1a-A **1a**-B **1a**-C

Table S1. Single point energy[1] of the tautomeric forms of **1a**.

	Single point energy (Hartree)	Difference (Kcal mol^{-1})	HOMO (eV)	LUMO (eV)
1a-A	–1238.28400	0	6.15	2.93
1a-B	–1238.22218	38.8	6.02	3.14
1a-C	–1238.15535	80.7	5.00	4.08

1) B3LYP/6-31G(d) levels of theory. 1 Hartree = 27.2 eV = 627.51 Kcal mol^{-1}.

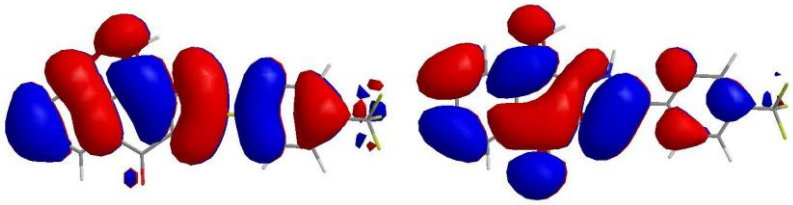

Figure S6-6. HOMO (6.02 eV: left) and LUMO (3.14 eV: right) of the tautomeric form of **1a**-B.

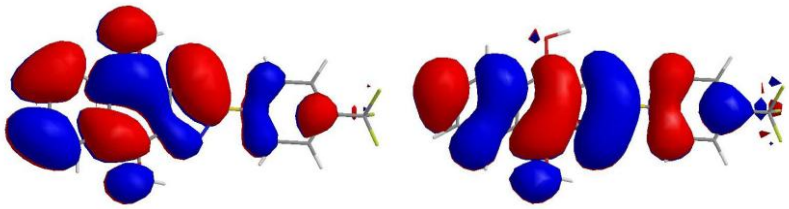

Figure S6-7. HOMO (5.00 eV: left) and LUMO (4.08 eV: right) of the tautomeric form of **1a**-C.

DFT calculations of the dimer form of 1a

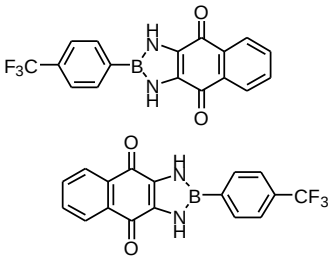

Table 2. Single point energy of the dimer forms of **1a**.

	Single point energy (Hartree)	HOMO (eV)	LUMO (eV)
Optimized **1a-1a**' [1] (Input CIF)	–2476.58964	6.11	3.16
Dimer **1a-1a**' (CIF)	–2476.24639	6.18	3.11
Monomer **1a** (CIF)	–1238.11350	6.21	2.92

1) B3LYP/6-31G(d)//B3LYP/6-31G(d) level of theory.

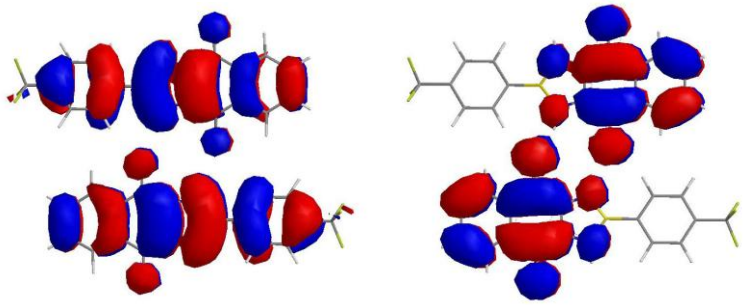

Figure S6-8. HOMO (6.11 eV: left) and LUMO (3.16 eV: right) of the dimer form of **1a-1a** optimized at B3LYP/6-31G(d) level using the CIF file as input.

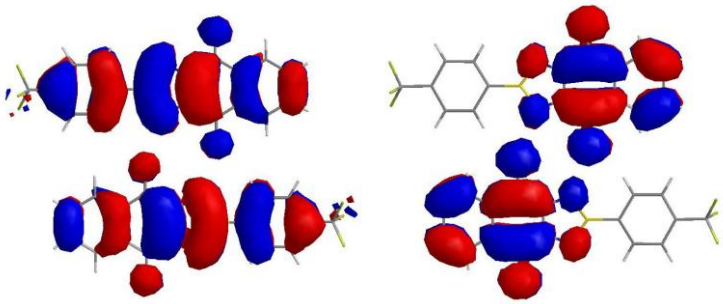

Figure S6-9. HOMO (6.18 eV: left) and LUMO (3.11 eV: right) of the dimer form of **1a-1a** using the CIF file.

DFT calculation of 2,6-Diphenyl-1H,5H-pyrrolo[2,3-f]indole-4,8-dione

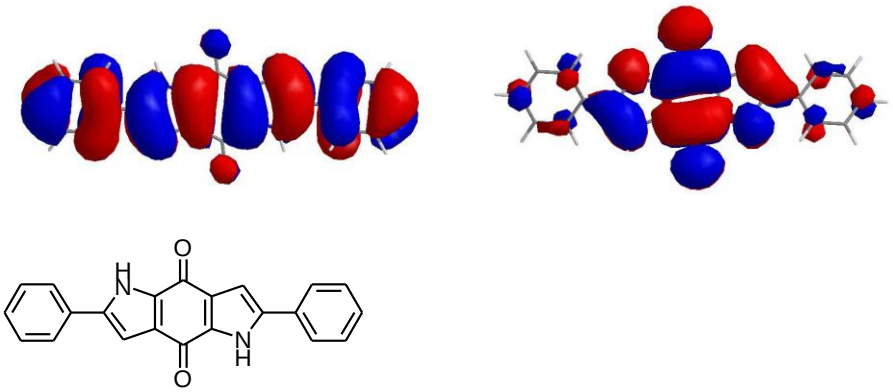

Figure S6-10. HOMO (5.58 eV: left) and LUMO (2.46 eV: right) of 2,6-Diphenyl-1H,5H-pyrrolo[2,3-f]indole-4,8-dione having an isoelectric structure.

7. FET characteristics

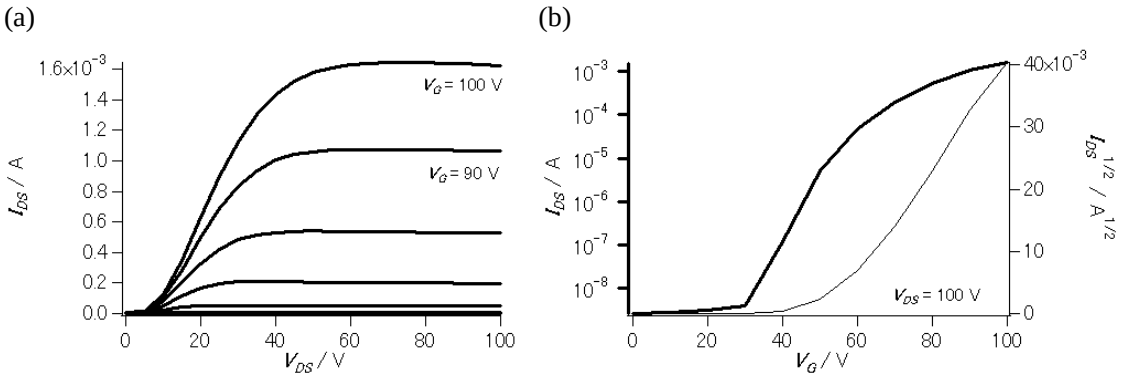

Figure S7-1. (a) Output characteristics of bottom-contact FET **1a** (T_{sub} = 20 °C, HMDS treated surface). (b) Transfer characteristics of the same device **1a** (right). The mobility calculated in the saturation regime is 8.8×10^{-3} cm^2 V^{-1} s^{-1}.

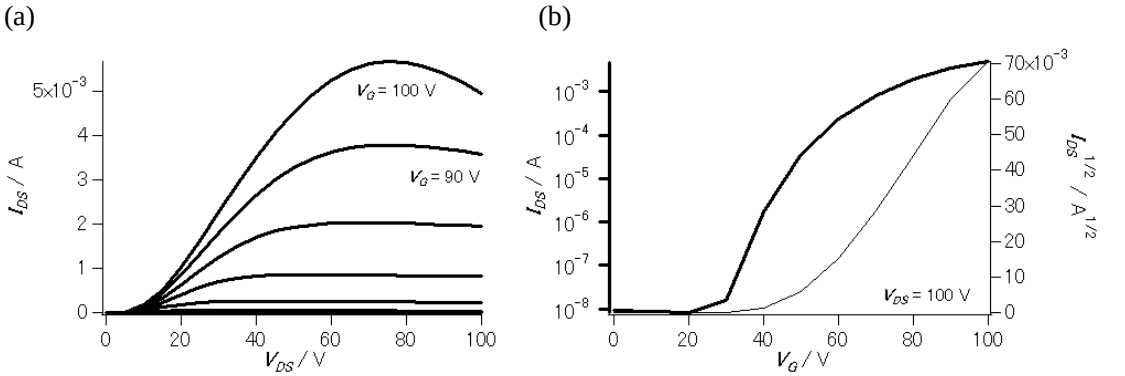

Figure S7-2. (a) Output characteristics of bottom-contact FET **1a** (T_{sub} = 100 °C, HMDS treated surface). (b) Transfer characteristics of the same device **1a** (right). The mobility calculated in the saturation regime is 3.9×10^{-2} cm^2 V^{-1} s^{-1}.

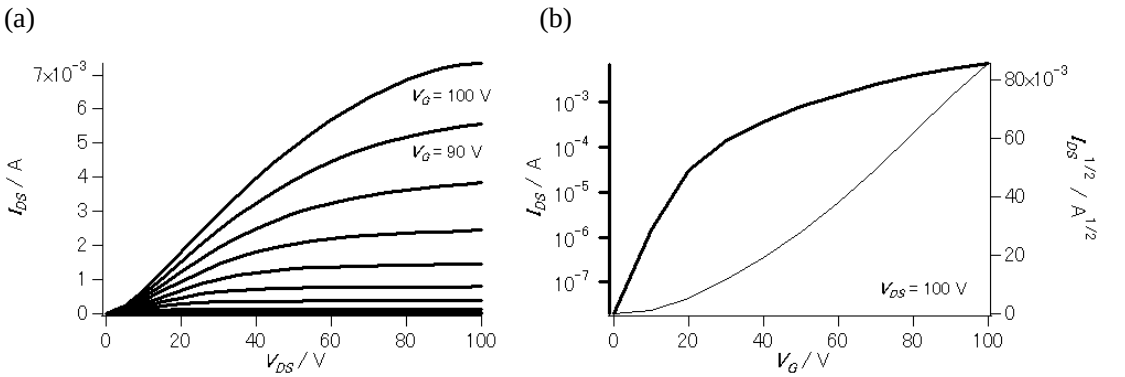

Figure S7-3. (a) Output characteristics of bottom-contact FET **2** (T_{sub} = 20 °C, HMDS treated surface). (b) Transfer characteristics of the same device **2** (right). The mobility calculated in the saturation regime is 3.7×10^{-2} cm^2 V^{-1} s^{-1}.

Table S3. Air stability of a bottom-contact FET **2**.

compd.	T_{sub} (degree)	mobility (cm^2/Vs)	on/off	threshold (V)
2 (in vacuo)	20	n: 3.7×10^{-2}	6×10^5	+38
2 (air 1 h)		n: 3.3×10^{-3}	3×10^4	+16
2 (air 1 d)		n: 8.3×10^{-6}	2×10^4	+10

(a) (b)

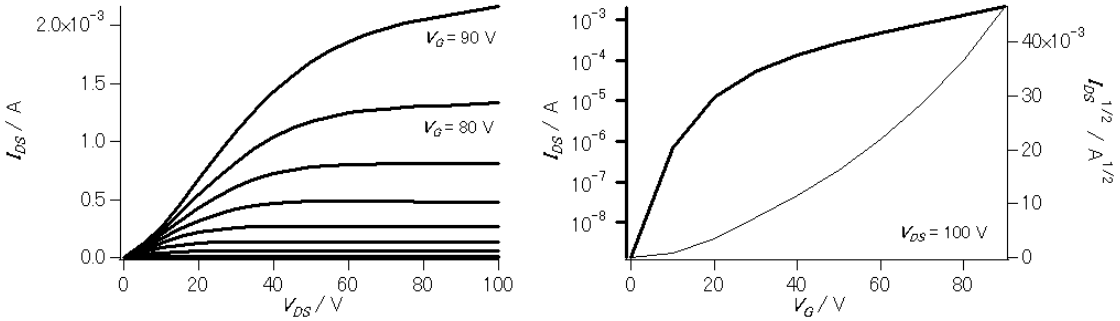

Figure S7-4. (a) Output characteristics of bottom-contact FET **3b** (T_{sub} = 20 °C, HMDS treated surface). (b) Transfer characteristics of the same device **3b**. The mobility calculated in the saturation regime is 1.5×10^{-2} cm^2 V^{-1} s^{-1}.

(a) (b)

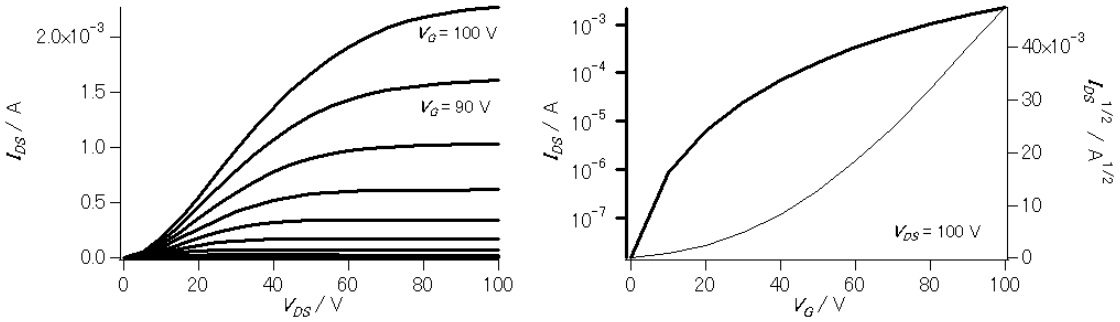

Figure S7-5. (a) Output characteristics of bottom-contact FET **3b** (T_{sub} = 50 °C, HMDS treated surface). (b) Transfer characteristics of the same device **3b**. The mobility calculated in the saturation regime is 7.8×10^{-3} cm^2 V^{-1} s^{-1}.

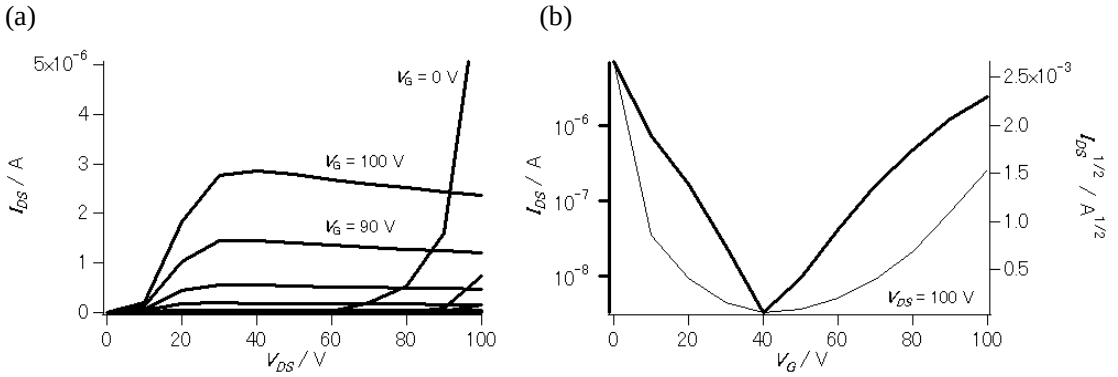

Figure S7-6. (a) n-Type output characteristics of **3c** and (b) transfer characteristics of **3c** (T_{sub} = 20 °C, HMDS treated surface). The mobility calculated in the saturation regime is 2.3×10^{-5} cm^2 V^{-1} s^{-1}.

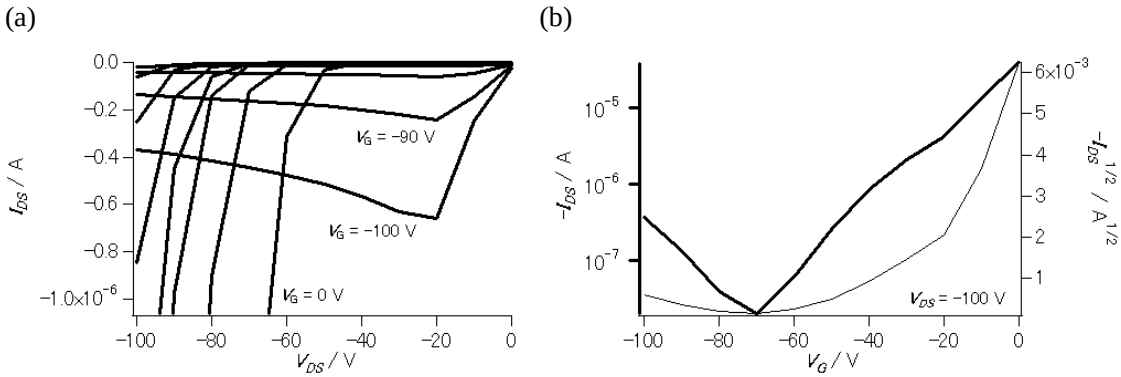

Figure S7-7. (a) p-Type output characteristics of **3c** and (b) transfer characteristics of **3c** (T_{sub} = 20°C, HMDS treated surface). The mobility calculated in the saturation regime is 1.5×10^{-5} cm^2 V^{-1} s^{-1}.

8. XRD patterns

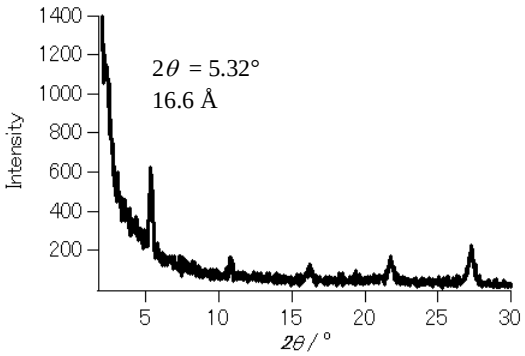

Figure S8-1. X-ray diffractogram of 50 nm films of **1a** at T_{sub} = 20 °C on HMDS treated surfaces.

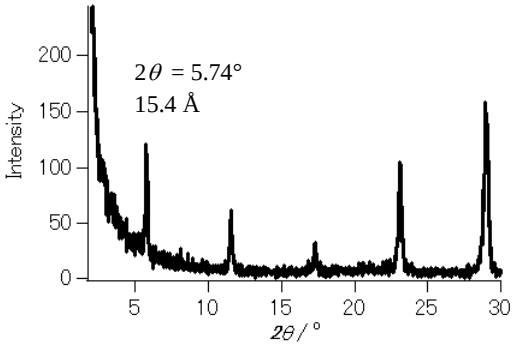

Figure S8-2. X-ray diffractogram of 50 nm films of **2** at T_{sub} = 20 °C on HMDS treated surfaces.

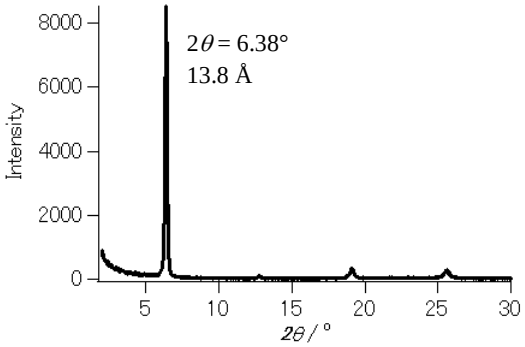

Figure S8-3. X-ray diffractogram of 50 nm film of **3a** deposited at T_{sub} = 20 °C on a HMDS treated surface.

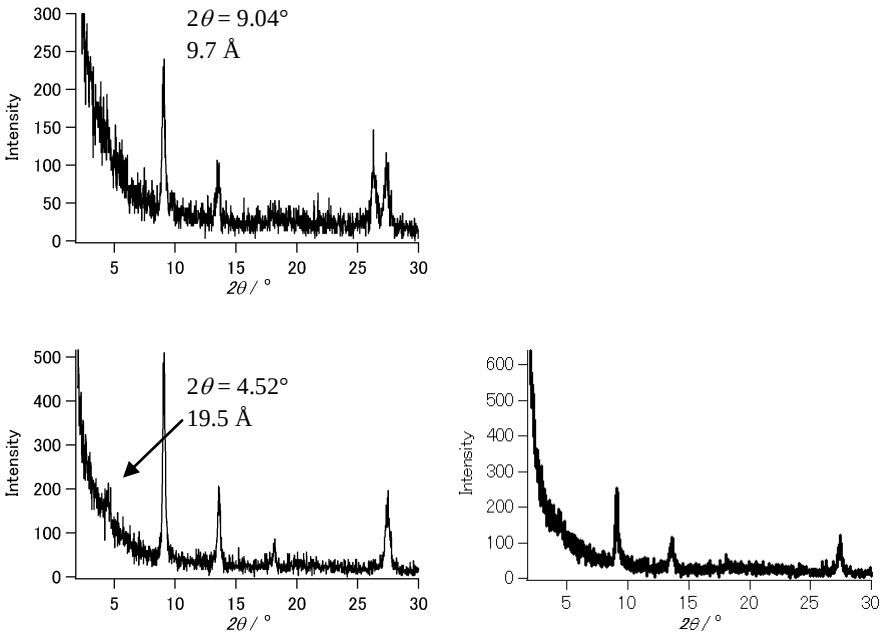

Figure S8-4. X-ray diffractograms of 50 nm films of **3b** deposited at T_{sub} = 20 °C on a HMDS treated surface (top), at 50 °C on a untreated surface (left) at 50 °C on a HMDS treated surface (right).

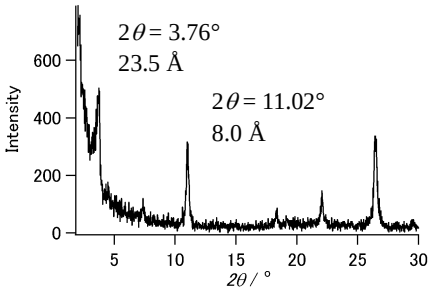

Figure S8-5. X-ray diffractogram of 50 nm film of **3c** deposited at T_{sub} = 20 °C on a HMDS treated surface.

9. AFM measurements

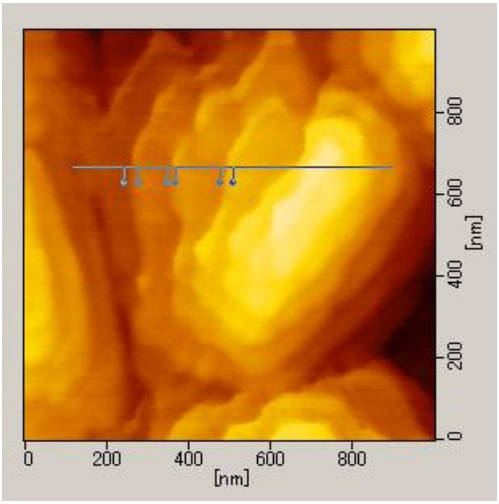

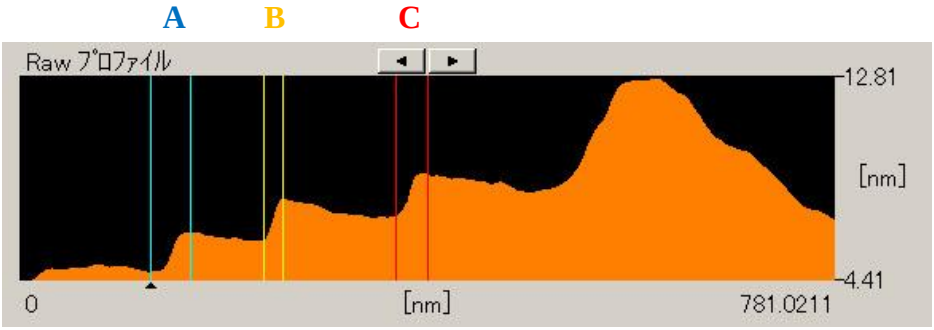

	Z1 [nm]	Z2 [nm]	Vertical interval [nm]	Distance [nm]	Angular difference
A	7.181	8.870	1.688	30.516	3.167
B	6.162	7.860	1.697	18.310	5.297
C	4.853	6.506	1.653	38.145	2.482

Figure S9-1. AFM images of 50 nm film of compound **1a** deposited at T_{sub} = 100 °C on a HMDS treated substrate.

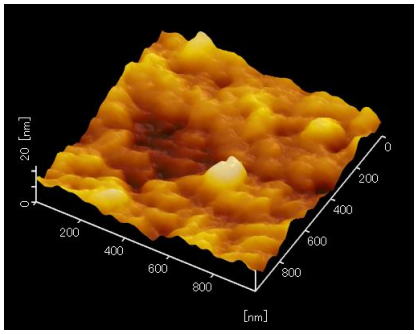

Figure S9-2. AFM image of 50 nm film of compound **3b** deposited at T_{sub} = 20 °C.